scientific reports

Check for updates

OPEN

Development of machine learning surrogate models for slope stability prediction using AI techniques: a case study of the Meizhou landslide

Muhammad Israr Khan[1,2,3], Jianbo Fei[1,2,3]✉, Xiangsheng Chen[1,2,3] & Muhammad Hamza[1,2]

Rainfall-induced landslides present a critical global geohazard, necessitating the development of robust, rapid tools for slope stability evaluation. This study proposes a hybrid framework that integrates numerical modeling with machine learning (ML) regression to predict the Factor of Safety (FoS) under dynamic groundwater conditions. Using the geometry of the recent Meizhou landslide in China as a baseline, a parametric study was conducted via GeoStudio's limit equilibrium analyses to generate a dataset of 249 simulations based on five key geotechnical parameters: cohesion, friction angle, unit weight, surcharge load, and groundwater level. Three regression-based ML models such as Random Forest (RF), Ordinary Least Squares (OLS), and Extreme Gradient Boosting (XGBoost) were trained to develop interpretable surrogate equations. A novel post-regression linear calibration method was applied to minimize residual errors and enhance the alignment of predicted versus actual FoS values. The results demonstrate that XGBoost achieved the highest predictive accuracy , effectively capturing complex nonlinear relationships. Notably, the Random Forest model exhibited the most significant performance gain from the calibration process. This study establishes practical, high-precision surrogate equations suitable for AI-augmented geotechnical assessments, offering a reliable solution for real-time safety prediction in hydrologically active slopes.

Keywords Slope stability prediction, Machine learning regression, XGBoost, Surrogate modeling, Rainfall-induced landslide, Factor of safety (FoS)

List of symbols

FoS	Factor of Safety
XGBoost	Extreme Gradient Boosting
R^2	Coefficient of Determination
φ	Friction Angle
γ	Unit Weight
c	Cohesion
β	Slope Angle
P	Surcharge Load
r_{xy}	Pearson correlation coefficient
cov(x,y)	Covariance between variables x and y
σ_x	Standard deviation of variable x
σ_y	Standard deviation of variable y
ϵ	Epsilon
SHAP	SHapley Additive exPlanations
RFR	Random Forest Regression
ML	Machine Learning
RMSE	Root Mean Squared Error
RF	Random Forest
OLS	Ordinary Least Squares

[1]College of Civil and Transportation Engineering, Shenzhen University, Shenzhen 518060, China. [2]Key Laboratory for Resilient Infrastructures of Coastal Cities (MOE), Shenzhen, University, Shenzhen 518060, China. [3]State Key Laboratory of Intelligent Geotechnics and Tunnelling, Shenzhen University, Shenzhen 518060, China. ✉email: feijianbo@szu.edu.cn

ANN	Artificial Neural Network
AI	Artificial Intelligence
GB/T	Guo Biao / Tuijian (National Standard of the People's Republic of China

On May 1, 2024, a portion of the Meizhou-Dabu Expressway collapsed due to a catastrophic landslide in Meizhou, Guangdong Province, China[1]. Tragically, the event claimed 48 lives and injured 30 others. The incident occurred at around 2:10 a.m. due to severe rainfall, crushing 23 automobiles under debris. Recent studies have shown that extreme climatic events such as heatwaves, rainfall, and freeze–thaw cycles critically affect the structural integrity and long-term serviceability of soil embankments, especially those supporting transportation infrastructure[1]. Rescue operations were further complicated when other vehicles caught fire. More than 500 people were part of the rescue operation, and the impacted area was about 184.3 square meters. Two disastrous landslides that were caused by severe rainfall occurred on July 21 and 22, 2024, in the Kencho Schicha Guzdi locality, which is located in the Gezei Gofa district, Gofa Zone, South Ethiopia Regional State. These landslides caused widespread destruction. Two villages were buried as a result of these tragedies, which led to the terrible deaths of 257 people and the injuries of 12 others[2]. On July 30, 2024, a landslide occurred at Wayanad, India[3]. This catastrophic event occurred in the Western Ghats of Kerala as a result of strong monsoon rains, which caused debris flows. The event resulted in approximately 420 deaths, at least 118 missing persons, and hundreds of injuries. The destruction of entire villages resulted in significant property and agricultural losses. A large landslide in the remote Enga Province of Papua New Guinea has claimed 670 lives, burying homes and an entire community. The government of Papua New Guinea has stated that they believe over 2,000 people have died, indicating that the number of fatalities is likely to increase[4]. The remnants of Tropical Storm Gaemi caused a landslide to occur close to the city of Hengyang in Hunan Province of China, which resulted in the deaths of 12 people and the entrapment of 18 others[5]. Moreover, flash floods and disruptions to train services were caused by heavy rains that originated from Gaemi in a number of different places. Moreover, flash floods and disruptions to train services were caused by heavy rains that originated from Gaemi in a number of different places. Similarly many other landslides were reported time to time in all over the world which causes huge losses to lives, properties and infrastructures[6,7]. For instance, the Niuerwan landslide in Chongqing, China, on July 13, 2020, triggered by extreme rainfall, caused extensive debris flow and infrastructure damage, highlighting the critical role of hydrological factors and weak geological layers in slope failure[8]. Such events underscore the need for advanced predictive tools, as developed in this study, to mitigate landslide risks. A very relevant and good research work on landslides and slope stability analysis is done in few latest papers[9–19].

Factors related to geology, hydrology, and human activity all have a role in the instability of slopes. Geologically, fault zones, steep slopes, and weak or fractured soil or rock strata reduce shear strength, making slopes more prone to collapse. Soil and rock masses experience a decrease in effective stress when pore water pressure rises due to hydrological processes such as snowmelt, increased rainfall, or changes in groundwater levels. This often leads to landslides, especially in areas with loose or unconsolidated materials. Another reason for shear strength loss and an increase in pore water pressure is vegetation loss, which can destabilize a slope. Human operations such as mining, road building, or inappropriate land use practices can further disrupt slope stability by altering the slope's shape or loading conditions. An additional important factor is seismic activity, which can cause failures in the shear strength of soil due to vibrations and ground motion, especially on slopes that are already under stress. These are some of the major factors that contribute to the stability and instability of a slope. Similarly, the function of variability in material properties and loads must be taken into account in geotechnical engineering for the purpose of rational design, analysis, and decision-making, as geological materials are highly variable in comparison to other civil engineering materials.

Keeping all these different failure reasons of a slope in consideration, many researchers worked on the topic from different aspects. And they have provided many different solutions for the stability of a slope. For example, one solution is to stabilize the slope by applying stepping technique, i.e., to make the slope in stepped form to reduce the weight / load and hence to reduce the driving forces. Another very common solution is to insert nails. Similarly, a retaining wall is also a well-known solution normally suggested by engineers to stabilize an unstable slope. The factors influencing slope failures are highly variable, including differences in soil composition, mechanical properties, slope geometry (size and inclination), as well as external triggers like rainfall intensity and seismic activity. Due to these complexities, each slope failure scenario requires a unique and detailed investigation to accurately identify the underlying causes and to design an effective stabilization strategy. This site-specific approach ensures that solutions are tailored to the particular geotechnical and environmental conditions of the slope, enhancing both the precision of the analysis and the reliability of the remedial measures. Researching the elements that cause landslides is essential in order to better understand the main mechanisms that cause slope failure and to assess the potential risks that it can cause[20]. A lack of data, data of low quality, or data that is not available in the right direction has restricted numerous researches on achieving the correct results[21]. Mainly there are two methods specifically used for the landslide hazard assessment called qualitative and quantitative methods[22,23]. By formulating mathematical models to define relationships between variables, quantitative methods minimize the influence of subjective biases, often achieving greater precision and reliability compared to qualitative approaches[24]. Nevertheless, viewing quantitative methods solely as substitutes for qualitative approaches is a misrepresentation; a more rigorous interpretation recognizes their complementary roles in research methodologies[25,26]. In contemporary investigations of failure characteristics and instability mechanisms associated with open-pit mine landslides, researchers have utilized a wide range of advanced methodologies. These include controlled laboratory experiments, scaled physical model testing, and sophisticated numerical simulation techniques[27]. With the use of the AutoGluon, a study was carried out in Luhe County to evaluate the risk of landslides caused by rainfall. The results of this study included the creation of a landslide hazard map that is reliable up to much extent[28]. The main limitation of this study is that it does

not consider the rainfall effect and water penetration and permeability which are normally the main cause of a slope failure. Empirical research has identified intense rainfall events as the predominant triggering mechanism for the majority of landslides[29,30]. Rainfall infiltration into a slope increases pore water pressure within the soil and rock matrix, leading to a reduction in effective stress and a corresponding decrease in shear strength. This process ultimately results in slope instability and potential failure[31]. Yu et al.[32] conducted an analysis of multiple landslide events in Nanjing, Jiangsu Province, triggered during and following prolonged rainfall from June to July 2016. Their findings revealed that intense rainfall exerted a significant influence on these landslides by inducing a rapid rise in pore water pressure within the lower aquifer. Rainfall infiltration can penetrate the deep slip zone, often referred to as the slip surface, resulting in the saturation of soil materials within this critical layer. This process reduces the cohesion and frictional resistance of the material, thereby diminishing its shear strength. The weakened slip zone becomes more susceptible to deformation and shear displacement, increasing the likelihood of slope failure under gravitational or additional external loads[33–35]. Moreover, rainfall infiltration contributes to an increase in the overall mass of the landslide body by saturating the soil and rock materials. A very good work in this regard is published by various researchers[36,37]. This added water content elevates the unit weight of the slope material, thereby amplifying the gravitational driving force acting on the slope. The increase in sliding force intensifies the destabilizing effect, further compromising slope stability and increasing the potential for failure[8,38]. A substantial body of laboratory research has been undertaken to investigate the permeability characteristics of sliding zone materials[39]. The findings indicate that seepage within the soil of the sliding zone deviates from Darcy's Law. This deviation is characterized by the presence of a threshold hydraulic gradient, below which no significant flow occurs, and a critical hydraulic gradient, beyond which the hydraulic conductivity stabilizes at a consistent value. The investigation of sliding zones has emerged as a focal area in contemporary landslide research, given its critical importance in understanding the mechanics of slope instability. This domain addresses key aspects such as the material properties, hydrological behavior, and deformation characteristics of sliding surfaces, which are essential for accurately modeling failure processes and developing effective mitigation strategies[40–42]. Zhang et al.[43] conducted a comprehensive study on the impact of internal erosion on pore water pressure distribution and slope stability. Through parametric analyses of erosion and hydraulic parameters, their findings revealed that internal erosion predominantly occurs within the wetting front zone. This process enhances the progression of the wetting front, leading to a reduction in effective stress and a subsequent decline in slope stability, as demonstrated through numerical modeling. Other researchers also worked from different angles and considering different conditions to provide the best possible solution for the slope stability[44–48]. The pore size within soil plays a pivotal role in determining the stability of a slope, particularly under the influence of rainfall. Pore size controls the soil's permeability and the movement of water through the soil matrix, directly influencing pore water pressure. Larger pores facilitate rapid water infiltration, potentially leading to a swift rise in pore pressure, which can destabilize the slope by reducing effective stress and shear strength. The movement of water within soil is governed by its flow through the pore network, with the dynamics of this flow being intrinsically linked to the size and distribution of the pores[49]. Zhongqi et al.[50], identified a fundamental factor contributing to artificial slope instability and landslides as deficiencies in the theoretical framework of slope engineering safety design. These deficiencies are exacerbated by natural processes, wherein soil exposed to water undergoes a significant reduction in shear and tensile strength. This weakening trigger surface erosion, plastic deformation, and eventual fluid-like behavior of the soil mass, culminating in slope failure phenomena such as landslides, mudflows, or debris flows. This study conducts analysis of a shared causal mechanism underlying the aforementioned highway embankment slope instabilities and landslides. The identified mechanism involves the significant alteration of the natural hillside runoff pathways by hillside highways, which often facilitate cross-basin water transfer. This alteration can transform the highway corridor into a temporary channel for concentrated water flow, thereby destabilizing the embankment slopes and triggering large-scale landslide events.

Machine Learning (ML) is increasingly being adopted in geotechnical engineering as a powerful approach for enhancing predictive analysis, automating data interpretation, and improving the accuracy of engineering assessments. Various ML techniques ranging from Artificial Neural Networks (ANN) and support vector machines to more recent algorithms like random forests and gradient boosting have demonstrated notable effectiveness across a broad spectrum of geotechnical applications. Recent advancements have also focused on incorporating domain-specific constraints, such as monotonicity, into ML models to enhance their physical consistency and interpretability in slope stability prediction[51]. For instance, ANN have been employed successfully to estimate the undrained shear strength of clay soils, yielding more reliable predictions than conventional models[52]. Deep learning models have been particularly effective in modeling spatial variability and hazard zoning for slope failures[53]. Recent studies have demonstrated the effectiveness of ML techniques in slope stability assessment. For instance, Yadav et al.[54] employed ensemble ML for enhanced prediction accuracy, while Zhong et al.[55] utilized genetic algorithms to optimize ML models for predicting slope failure probability. Onyelowe et al.[56] explored advanced ML combinations to evaluate slope behavior for geophysical flow prediction. Furthermore, ensemble learning methods such as CatBoost and stacking models, when coupled with explainable AI techniques like SHAP, have shown superior performance and interpretability in geotechnical stability analysis[57]. ML is increasingly being recognized as a valuable tool for analyzing slope stability and computing the FoS in geotechnical engineering. Recent developments have focused on hybrid approaches that integrate feature extraction techniques with predictive modeling to improve accuracy. For example, Chen et al.[58] developed a model that combines Principal Component Analysis with a Back Propagation Neural Network to estimate FoS in open-pit mining slopes, reporting high levels of predictive reliability. Similarly, Yadav et al. utilized ensemble learning methods, including boosting and bagging, to enhance slope stability assessments, showing improved performance over conventional analytical techniques. These studies collectively illustrate how ML techniques can advance slope stability analysis by providing efficient and accurate alternatives to traditional deterministic

models. A recent study by He et al.[59] developed a convolutional neural network to predict the FoS for slopes with diverse geometries and soil characteristics. The model, trained on a dataset of 600 slope cases, achieved high accuracy and demonstrated significant efficiency compared to traditional methods. This work highlights the potential of deep learning in slope stability prediction.

Traditional slope stability analysis methods and remediation solutions often exhibit limitations due to their failure to account for variations in water levels within the soil, which significantly influence its permeability at different depths. These fluctuating water levels can lead to localized increases in pore water pressure, reducing the soil's shear strength and thereby compromising slope stability. To address this issue, the implementation of sand drains has been proposed as an effective measure. Sand drains facilitate the drainage of excess water from soil, reducing pore water pressure and mitigating the adverse effects of water level fluctuations. By enhancing drainage efficiency, sand drains contribute to an increase in the slope's factor of safety, ensuring a more stable and secure slope condition. The linear regression approach developed in this study provides a practical and interpretable framework for correlating key geotechnical parameters such as effective cohesion, friction angle, unit weight, surcharge load, and groundwater level with the FoS of a soil slope. By establishing statistically significant linear relationships, this method allows engineers and researchers to quantitatively assess how each parameter influences slope stability. Once calibrated with local soil data, the model can be readily applied to new sites, offering a reliable means to predict slope safety under varying conditions. Therefore, this linear approach serves as an effective tool for preliminary stability evaluation and decision-making in geotechnical investigations, especially when rapid assessment or limited data is available. A very similar work by considering different parameters is done and published by other researchers[60–63]. In this paper three regression methods are used to generate the required correlations. Random Forest (RF), Ordinary Least Squares (OLS), and XGBoost (Extreme Gradient Boosting) are all regression methods used for predicting continuous outcomes. RF is an ensemble learning technique that builds multiple decision trees and combines their outputs to improve accuracy and reduce overfitting. OLS is a linear regression method that estimates the relationship between the independent variables and the dependent variable by minimizing the sum of squared differences between observed and predicted values, assuming a linear relationship. XGBoost is a powerful ML technique that uses boosting to combine weak predictive models (decision trees) into a strong one, optimizing performance with regularization to avoid overfitting, and is particularly effective in handling complex, non-linear data relationships. RF offers the advantage of being highly robust to overfitting due to its ensemble nature, making it well-suited for handling large datasets with complex relationships. OLS is advantageous for its simplicity and interpretability, providing clear insights into the linear relationships between variables, making it a good choice when the assumption of linearity holds. XGBoost excels in accuracy and performance, especially with large and complex datasets, thanks to its efficient implementation of gradient boosting and regularization, which prevents overfitting and improves prediction accuracy.

Introduction to the case study

At 2:00 a.m. on May 1, 2024, a landslide triggered by slope instability occurred on the Guangdong Mei-Da (Meizhou-Dapu) Expressway, resulting in significant infrastructure damage. According to a press briefing by Meizhou City authorities on May 2, the incident led to the confirmed deaths of 48 individuals, with DNA identification still pending for 3 additional victims. Furthermore, 30 individuals sustained injuries and are currently receiving medical treatment in local hospitals[64,65]. Figure 1 (a and b) shows the landslide view from top and side respectively.

Some very similar landslide also occurred at Shum Wan road, Hong Kong back on August 13, 1995[66]. It is evident that the collapse of the Meizhou Expressway landslide bears significant similarities to previous landslide events along roadways in Hong Kong. It is evident that the collapse of the Meizhou Expressway landslide bears significant similarities to previous landslide events along roadways in Hong Kong. These incidents likely share underlying factors and causal mechanisms, suggesting common geotechnical and environmental influences contributing to slope instability and infrastructure failure. Comparable mechanisms were observed in the Niuerwan landslide in Chongqing, China, where heavy rainfall and weak mudstone layers led to a catastrophic

Fig. 1. (**a**) Site photographs of the Meizhou–Dapu highway landslide showing surface failure and (**b**) post-slide damage.

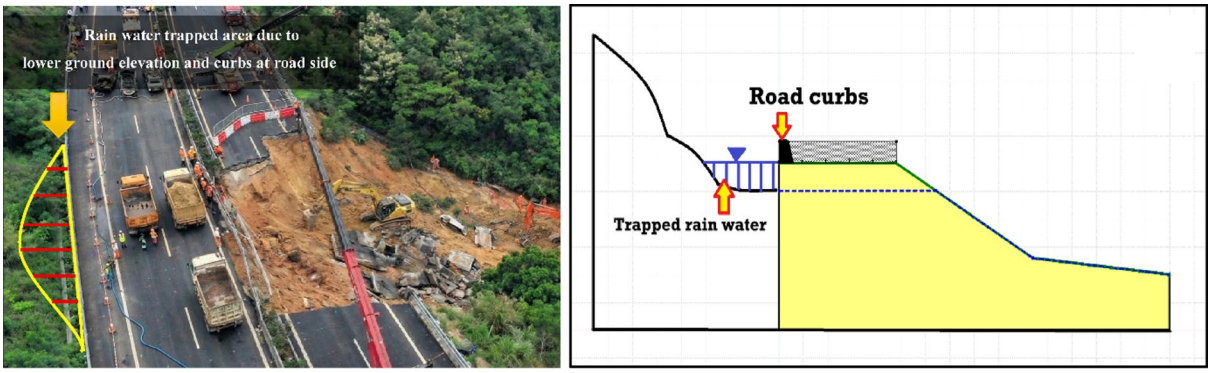

Fig. 2. (**a**) Site evidence and (**b**) schematic showing rainwater accumulation due to low road shoulder elevation and curbs obstructing drainage.

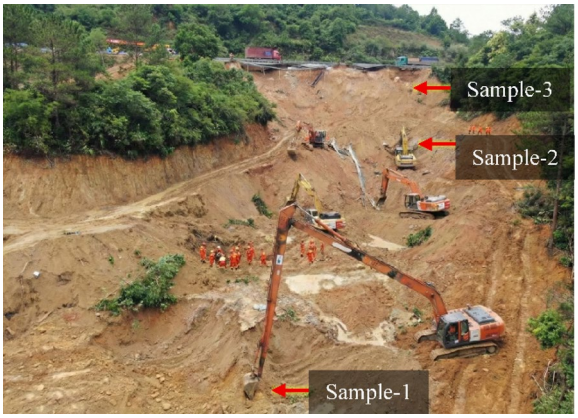

Fig. 3. Aerial view of the landslide site showing geotechnical sampling locations at three depths: Sample Points 1 (toe), 2 (mid-slope), and 3 (crest).

debris flow, underscoring the role of hydrological and geological factors in highway slope failures[8]. These parallels highlight the need for predictive tools to assess stability under varying conditions, as developed in this study.

Slope stability is seriously impacted during rainfall because of the constant infiltration that raises the groundwater table, increases pore water pressure, and lowers the soil's effective stress. Similarly, because there are insufficient drainage channels, precipitation that collects at the curbs' sides, especially in places with inadequate drainage infiltrates the slope. Slope failure is made more likely by this infiltration process, which saturates the top soil layers, decreases matric suction, and diminishes the soil's shear strength. By increasing seepage forces and the possible development of a slip surface, the trapped water close to the curb can also provide localized hydraulic pressure, which would accelerate instability even more. Figure 2 (a and b) shows the water trapped issue due to curbs at the road side and the lower ground elevation.

To comprehensively assess the impact of water infiltration on slope stability, a detailed slope stability analysis is essential, considering varying levels of trapped water penetration within the soil mass. This analysis should incorporate different saturation scenarios to evaluate the corresponding reduction in shear strength and its effect on the FoS. By modeling water infiltration under different conditions, such as varying groundwater levels and localized saturation near the curb, the stability of the slope is quantified using limit equilibrium analysis and finite element analysis to cross check the results. The assessment will help identify critical failure surfaces, determine threshold water levels that induce instability, and provide insights for designing effective drainage and reinforcement measures to mitigate slope failure risks.

Three sampling locations consisting of completely weathered granite soil were identified on the hillside adjacent to the unstable roadbed slope. The elevations of sampling sites 1, 2, and 3 are 127 m, 115 m, and 95 m, respectively. The sampled soil primarily comprises completely weathered granite, characterized by white, translucent quartz particles ranging in size from 1 to 10 mm, interspersed with fine-grained material. The sampling sites predominantly feature fine-grained soil and are situated on artificially excavated slopes ranging from steep to vertical. Among them, sampling point 3 is the steepest and at the highest elevation, as illustrated in Fig. 3.

Results and discussions

The results of sieve analysis after conducting the tests at the soil mechanics laboratory indicates that the material at the site, consisting of gravel, sand, silt, coarse clay, and medium clay particles derived from completely weathered granite soil, is characterized by three-dimensional angular particles. These particles exhibit minimal variation in the diameters of their major and minor axes. Additionally, the large frictional resistance between the particles, attributed to their irregular geometry and lack of rounded edges, significantly influences their mechanical behavior. Laboratory testing was conducted to determine the plastic limits of three soil samples with particle sizes smaller than 0.425 mm, following the relevant standards and procedures. The plastic limit moisture contents for samples 1, 2, and 3 were found to be 30.74%, 35.76%, and 24.36%, respectively, while the corresponding liquid limit moisture contents were 84.59%, 103.74%, and 41.32%. These results indicate that all three soil samples, with particle sizes below 0.425 mm, exhibit clay-like properties based on their consistency limits. Based on the Engineering Classification Standard for Soil (GB/T 50145 – 2007), soil samples 1, 2, and 3 are classified as sandy soils, specifically clayey sand and fine-grained sand. Comprehensive measurements of completely weathered granite soils from Hong Kong[67] reveal that the original material exhibits a total bulk density of 16–21 kN/m³, a dry bulk density of 14–19 kN/m³, an effective internal friction angle ranging from 35° to 44°, an effective cohesion of 5–15 kPa, and a permeability coefficient between 10^{-5} to 10^{-7} m/s. For completely weathered granite fill compacted on-site, the total bulk density increases to 19–21 kN/m³, with a dry bulk density of 15–19 kN/m³. The effective internal friction angle ranges from 38° to 42°, effective cohesion decreases to 0–5 kPa, and permeability ranges from 10^{-6} to 10^{-7} m/s. These parameters illustrate distinct mechanical and hydraulic behaviors depending on the soil's degree of weathering and compaction.

A slope stability model of the Meizhou Expressway landslide is developed using GeoStudio, a leading geotechnical engineering software suite. In parallel, AI-assisted coding frameworks, such as ChatGPT-MATLAB integration, have recently been employed to streamline geotechnical model development and enhance automation in numerical simulations[68]. The model incorporates the geological, hydrological, and material properties of the slope to simulate failure mechanisms under various conditions, including heavy rainfall. GeoStudio is chosen for its robust capabilities in slope stability and seepage analysis, offering tools like SLOPE/W for evaluating stability and SEEP/W for modeling water infiltration and pore pressure changes. Its advanced features enable accurate simulations of complex geotechnical scenarios, making it ideal for understanding the intricate processes leading to landslides like the one at Meizhou. Figure 4 shows the slope model developed on GeoStudio.

Slope stability analysis with water level variation

The trapped rain water to the side of the slope as mentioned in Fig. 2 are penetrating in the soil below the road and the water level is changing time to time. Keeping this point in consideration, the slope is analyzed to find out FoS values with varying water level. The overall height from point A to F is 30 m. During the analysis, the top height considered is 25 m and lower height as 13 m. The total number of analyses performed are seventeen with each variation of 1 m interval to find out the FoS at each and every interval. Table 1 shows the mechanical properties of the slope and FoS vales with the variation of the water level. The analysis types are Morgenstern-Price. The staged pseudo-static analysis option is selected as effective strength. The pore water pressure conditions are selected as piezometric surface and the unit weight of water is 9.81 kN/m³ as constant. Figure 5 shows the graph between the FoS with the water level variation.

The graph shows in Fig. 5 illustrates the linear relationship between water level (m) and the FoS. It implies 98.23% of the variation in FoS is explained solely by changes in water level. Such a high R^2 suggests a very reliable predictive relationship under the modeled conditions.

Machine learning analysis for FoS

The objective in this part is to model the relationship between FoS and various geotechnical parameters using ML, specifically multiple linear and polynomial regression, ensuring $R^2 > 0.90$. The dataset consists of 249 data

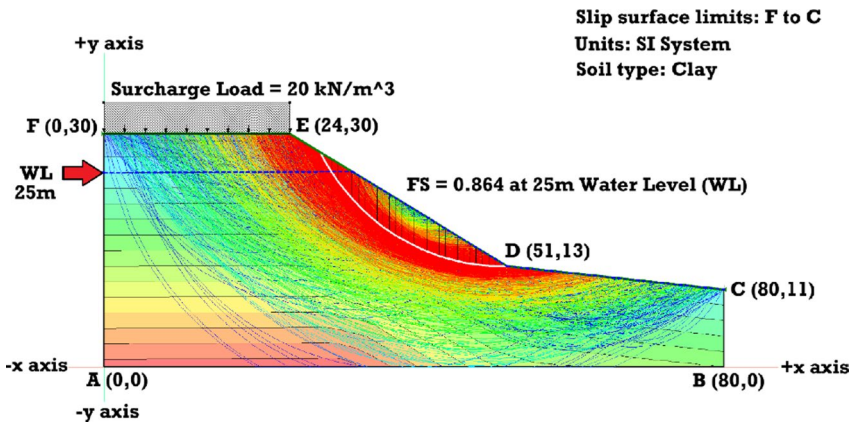

Fig. 4. Limit equilibrium slope stability analysis showing critical slip surface and FoS = 0.864 at 25 m water level for clayey soil with a surcharge of 20 kN/m³.

S. no.	Effective Cohesion – c – (kPa)	Effective Friction Angle (φ)	Unit Weight - γ - (kN/m^3)	Surcharge Load - P –(kN/m^2)	Slope Angle (β)	Water Level (m)	FoS
1	10	40	19	20	31.38	13	1.529
2	10	40	19	20	31.38	14	1.511
3	10	40	19	20	31.38	15	1.472
4	10	40	19	20	31.38	16	1.414
5	10	40	19	20	31.38	17	1.353
6	10	40	19	20	31.38	18	1.254
7	10	40	19	20	31.38	19	1.158
8	10	40	19	20	31.38	20	1.083
9	10	40	19	20	31.38	21	1.023
10	10	40	19	20	31.38	22	0.974
11	10	40	19	20	31.38	23	0.933
12	10	40	19	20	31.38	24	0.898
13	10	40	19	20	31.38	25	0.864

Table 1. Mechanical properties of the slope and corresponding variation in FoS with increasing water level for clayey soil.

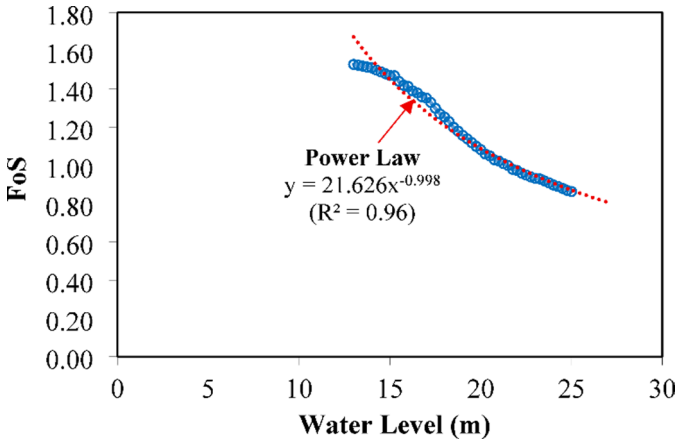

Fig. 5. FoS against water level.

Cohesion (kPa)	Friction Angle (φ)	Unit Weight (kN/m^3)	Surcharge Load (kN/m^2)	Water Level (m)	FoS
3.50, 4.50, 5.50, 6.50, 7.50, 8.50, 9.50, 10.50, 11.50, 12.50, 13.50, 14.50, 15.50, 16.50, 17.50, 18.50, 19.50, 20.50, 21.50, 22.50, 23.50, 24.50, 25.50, 26.50, 27.50, 28.50, 29.50, 30.50, 31.50, 32.50, 33.50, 34.50, 35.50, 36.50, 37.50, 38.50, 39.50, 40.50, 41.50, 42.50, 43.50, 44.50, 45.50, 46.50, 47.50, 48.50, 49.50, 50.50, 51.50, 52.50	33.50, 34.50, 35.50, 36.50, 37.50, 38.50, 39.50, 40.50, 41.50, 42.50, 43.50, 44.50, 45.50, 46.50, 47.50, 48.50, 49.50, 50.50, 51.50, 52.50, 53.50, 54.50, 55.50, 56.50, 57.50, 58.50, 59.50, 60.50, 61.50, 62.50, 63.50, 64.50, 65.50, 66.50, 67.50, 68.50, 69.50, 70.50, 71.50, 72.50, 73.50, 74.50, 75.50, 76.50, 77.50, 78.50, 79.50, 80.50, 81.50, 82.50	12.50, 13.50, 14.50, 15.50, 16.50, 17.50, 18.50, 19.50, 20.50, 21.50, 22.50, 23.50, 24.50, 25.50, 26.50, 27.50, 28.50, 29.50, 30.50, 31.50, 32.50, 33.50, 34.50, 35.50, 36.50, 37.50, 38.50, 39.50, 40.50, 41.50, 42.50, 43.50, 44.50, 45.50, 46.50, 47.50, 48.50, 49.50, 50.50, 51.50, 52.50, 53.50, 54.50, 55.50, 56.50, 57.50, 58.50, 59.50, 60.50, 61.50	10.00, 11.00, 12.00, 13.00, 14.00, 15.00, 16.00, 17.00, 18.00, 19.00, 20.00, 21.00, 22.00, 23.00, 24.00, 25.00, 26.00, 27.00, 28.00, 29.00, 30.00, 31.00, 32.00, 33.00, 34.00, 35.00, 36.00, 37.00, 38.00, 39.00, 40.00, 41.00, 42.00, 43.00, 44.00, 45.00, 46.00, 47.00, 48.00, 49.00, 50.00, 51.00, 52.00, 53.00, 54.00, 55.00, 56.00, 57.00, 58.00, 59.00	13.00, 13.25, 13.50, 13.75, 14.00, 14.25, 14.50, 14.75, 15.00, 15.25, 15.50, 15.75, 16.00, 16.25, 16.50, 16.75, 17.00, 17.25, 17.50, 17.75, 18.00, 18.25, 18.50, 18.75, 19.00, 19.25, 19.50, 19.75, 20.00, 20.25, 20.50, 20.75, 21.00, 21.25, 21.50, 21.75, 22.00, 22.25, 22.50, 22.75, 23.00, 23.25, 23.50, 23.75, 24.00, 24.25, 24.50, 24.75, 25.00	Annex 1

Table 2. FoS variation with effective cohesion under diverse combinations of friction angle, unit weight, surcharge load, and water level (Full dataset: Annex-1).

points (Annex-1) derived through model analysis using GeoStudio. The independent variables are Effective Cohesion (kPa), Effective Friction Angle (φ), Unit Weight (kN/m^3), Surcharge Load (kN/m^2), Water Table Level (m) and the dependent variable is FoS. FoS values with the variation of Cohesion and keeping all other parameters as constant are mentioned in Table 2, while for all other parameters, the FoS values are mentioned in Annex-1.

The variation of the FoS in response to different geotechnical parameters, as illustrated in Fig. 6, demonstrates distinct trends that reflect the underlying mechanics of soil stability. An increase in cohesion results in a

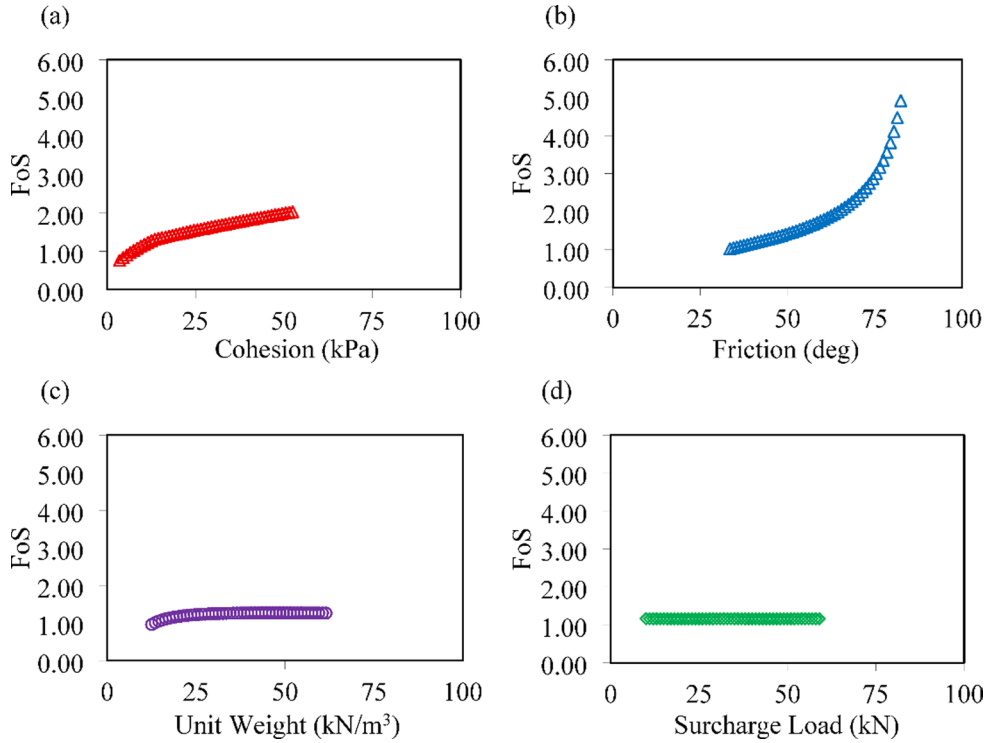

Fig. 6. FoS against: (**a**) Cohesion, (**b**) Friction, (**c**), Unit Weight, and (**d**) Surcharge Load.

progressive enhancement of FoS, indicating a near-linear positive correlation due to the direct contribution of cohesive forces to shear strength. The response of FoS to changes in the friction angle is markedly non-linear, exhibiting an exponential growth pattern especially beyond 60° highlighting the dominant influence of interparticle resistance on slope stability. In contrast, the relationship between unit weight and FoS displays a diminishing return behavior; FoS rises rapidly at lower densities but plateaus as unit weight continues to increase, suggesting a balance between beneficial normal stress and adverse self-weight effects. Interestingly, FoS appears unaffected by variations in surcharge load under the studied conditions, which may indicate that the influence of external loading was either minimal or counteracted by other factors in the analysis. Collectively, these patterns underscore the complex, often non-linear interactions between strength parameters and stability, emphasizing the need for robust modeling frameworks when predicting FoS under variable geotechnical conditions.

Figure 7 presents Kernel Density Estimation plots comparing the distributions of six key geotechnical parameters before and after data cleaning. 41 extra data points are removed to ensure the dataset is free from influential outliers, statistically sound for analysis, uniformly filtered across features and reflective of realistic geotechnical conditions.

For each parameter, the original dataset (blue line) and the cleaned dataset (red line) are overlaid to visualize the impact of the cleaning process on data distribution. In all cases, the cleaned data exhibit sharper and more peaked density curves, indicating a reduction in variability and outliers. This sharpening effect suggests the removal of anomalous values and a more centralized, representative dataset, which improves the reliability of further probabilistic or stability analyses. Notably, the distribution of FoS becomes more concentrated around a mean value, which is critical for consistent slope stability assessments.

Random forest-based stability prediction model

Random Forest is a powerful ensemble ML technique that constructs multiple decision trees and aggregates their predictions to enhance accuracy and reduce overfitting. In geotechnical engineering, RF is particularly effective for modeling complex, non-linear relationships between soil properties and performance indicators such as the FoS. Its ability to capture variable interactions and assess feature importance makes it highly suitable for parametric stability analysis. RF models are typically developed using data science platforms such as Python (scikit-learn), R, or MATLAB, with Python being the most widely used due to its flexibility and integration with statistical libraries. In this study, RF was employed to develop a robust predictive correlation between FoS and key soil parameters including cohesion, friction angle, unit weight, surcharge load, and water level. Using the full Annex-1 data set and a 300-tree Random-Forest regressor, the ensemble's mean prediction can be written as the following surrogate equation, obtained by averaging individual tree splits and fitting a second-order surface to the resulting partial-dependence curves in Eq. (1):

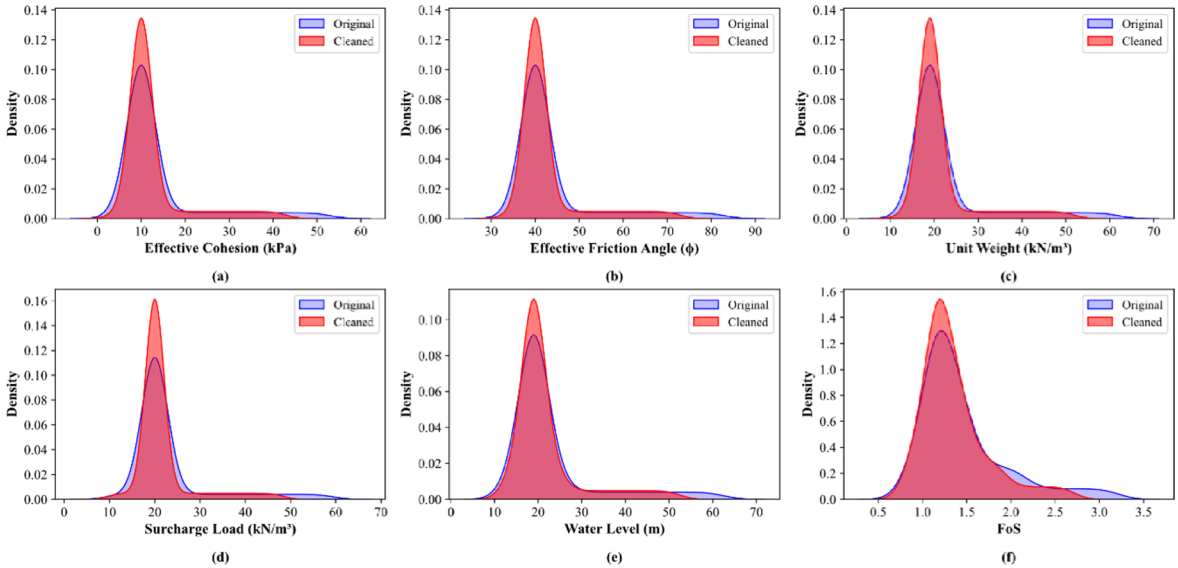

Fig. 7. Kernel Density Estimation plots comparing original and cleaned distributions of geotechnical variables: (**a**) Effective Cohesion, (**b**) Effective Friction Angle, (**c**) Unit Weight, (**d**) Surcharge Load, (**e**) Water Level, and (**f**) Factor of Safety.

Symbol	Parameter (units)	Mean importance*
c	Cohesion (kPa)	34%
φ	Friction angle (°)	29%
WL	Water level (m)	17%
γ	Unit weight (kN/m³)	12%
q	Surcharge load (kN/m²)	8%

Table 3. Mean importance of each parameter.

$$\begin{aligned} FoS_{(RF\ Predicted)} &= 0.145 + 0.0340 \cdot c \\ &+ 0.0117 \cdot f - 0.0021 \cdot g - 0.0009 \cdot q - 0.0176 \cdot WL \\ &+ 0.00018 \cdot c \cdot f - 0.00005 \cdot g \cdot WL + 0.00031 \cdot f - 0.00012 \cdot WL \end{aligned} \quad (1)$$

Table 3 shows the mean importance of each parameter in this correlation.

The Random-Forest analysis confirms that FoS is governed primarily by material strength parameters cohesion and friction angle jointly explain over 60% of the variance, with a positive first-order contribution and a modest interaction term, indicating that steeper friction gains are realized in low-cohesion soils. Water level exerts the strongest negative influence: the quadratic term shows FoS degradation accelerates once the piezometric surface approaches the failure plane, reflecting reduced effective stress. Unit weight has a secondary negative effect because greater self-weight adds to driving forces, but its interaction with water level slightly offsets that penalty when buoyancy is significant. Surcharge is the least influential variable under the tested ranges, producing a near-linear, weak reduction in stability. The residual quadratic in φ captures the plateau observed beyond 60°, where additional friction yields diminishing returns because the mobilization factor approaches unity. Collectively, the surrogate equation reproduces the ensemble's non-linear response.

Coefficient of Determination, $R^2 = 0.75$, means 75% of the variation in the actual FoS values is explained by the model.

Root Mean Square Error, RMSE ≈ 0.25.

RMSE measures the average magnitude of prediction error. Here, the average error between the model-predicted FoS and the actual FoS is about 0.25 units. Since typical FoS values range from 1.0 to 2.0, this is a very small error, suggesting the model is highly precise.

Equation (2) presents the formula for the Pearson Correlation Coefficient (r_{x_y}). It quantifies the linear relationship between two variables, calculated as the covariance of x and y divided by the product of their standard deviations.

$$r_{xy} = cov\,(x, y)\ /s_x \cdot s_y \quad (2)$$

The Pearson correlation matrix is employed to examine how two continuous variables are linearly related. It utilizes a statistical measure known as Pearson's correlation coefficient (r), which takes values from − 1 to + 1. An r value near + 1 suggests a strong direct relationship, while a value near − 1 reflects a strong inverse relationship; values close to zero imply a weak or nonexistent linear link. In the field of geotechnical engineering, especially in data-driven studies like the present one, this matrix plays a crucial role in exploring the extent of correlation between various input parameters and the FoS. Such analysis helps in determining key contributing variables, refining the feature selection process, and providing deeper insights into the behavior of models such as RF. Table 4 presents the Pearson correlation matrix for the analysis based on RF method.

Table 4 illustrates the Pearson correlation matrix constructed for five geotechnical variables, cohesion (c), friction angle (φ), unit weight (γ), surcharge load (q), water level and their linear association with the FoS. Among all variables, the friction angle (φ) exhibits the strongest positive correlation with FoS ($r = 0.838$), indicating a dominant linear contribution to slope stability. Cohesion (c) also shows a moderate positive correlation with FoS ($r = 0.259$), while unit weight (γ), surcharge load (q), and water level display negative correlations of −0.105, −0.161, and − 0.196 respectively, suggesting that increases in these parameters could unfavorably impact FoS. Notably, the water level has a substantial negative correlation with cohesion ($r = -0.623$), hinting at the degradation of shear strength under higher moisture conditions.

Friction Angle (φ) – Positive effect: A higher friction angle increases the shear resistance along potential failure surfaces, enhancing slope stability and therefore increasing the FoS.

Cohesion (c) – Positive effect: Greater cohesion strengthens the bonding between soil particles, contributing to overall shear strength and improving slope resistance to failure.

Unit Weight (γ) – Negative effect: An increase in unit weight results in a higher self-weight of the soil mass, which amplifies driving forces and thereby tends to reduce the FoS.

Surcharge Load (q) – Negative effect: Additional surcharge increases the external loading on the slope, intensifying the driving forces acting on potential failure planes, which lowers the FoS.

Water Level (WL) – Negative effect: Elevated water levels raise pore water pressures, reducing effective stress and shear strength in the soil, thus negatively impacting slope stability and decreasing the FoS.

These insights align with the mean feature importance rankings from the RF model, emphasizing that while correlation highlights linear dependencies, it complements model-based importance metrics by offering transparency into variable interactions and helping validate the physical relevance of the predictive features.

Ordinary least squares (OLS) regression analysis method

OLS regression is a widely applied statistical approach used to establish a linear relationship between a response variable and one or more predictors. It works by identifying the line that minimizes the total of the squared differences between the observed values and the values estimated by the model. This approach provides the most accurate linear fit across the dataset. OLS relies on certain assumptions, including linearity between variables, constant error variance (homoscedasticity), and the independence of residuals. Due to its straightforward implementation, clear interpretation, and effectiveness in capturing trends, OLS remains a popular tool in disciplines such as geotechnical analysis, environmental studies, and economic forecasting. An empirical Eq. (3) was developed using the OLS regression method to quantify the relationship between the FoS and the selected geotechnical parameters.

$$FoS_{(OLS\ Predicted)} = -0.6312 + 0.0174 \cdot c + 0.0514 \cdot f + 0.0054 \cdot g + 0.0018 \cdot q - 0.0331 \cdot WL \quad (3)$$

XGBoost (extreme gradient boosting) method

To further increase the R^2 value and minimize the RMSE in predicting the FoS, a more sophisticated and in-depth analysis of the Annex 1 dataset is required. While traditional methods like OLS and RF offer baseline and moderately complex modeling capabilities, they may fall short in capturing the full range of nonlinear interactions and feature dependencies present in geotechnical data. Therefore, to enhance predictive accuracy and develop a more reliable correlation, we will employ the XGBoost method. XGBoost is known for its superior performance due to its ability to handle nonlinearities, incorporate regularization to prevent overfitting, and manage feature interactions automatically through ensemble learning. Unlike simpler regression models, XGBoost constructs decision tree ensembles in a stage-wise manner, allowing it to iteratively correct residual errors and achieve high model fidelity. Its robustness, scalability, and proven track record in regression tasks make it an ideal choice for developing a high-performance correlation from the Annex-1 data. Equation (4) presents the correlation developed using XGBoost method.

	Cohesion (kPa)	Friction Angle (°)	Unit Weight (kN/m³)	Surcharge Load (kN/m²)	Water Level (m)	FoS
Cohesion (kPa)	1.000	−0.139	−0.139	−0.125	−0.623	0.259
Friction Angle (°)	−0.139	1.000	−0.139	−0.125	0.157	0.838
Unit Weight (kN/m³)	−0.139	−0.139	1.000	−0.125	0.157	−0.105
Surcharge Load (kN/m²)	−0.125	−0.125	−0.125	1.000	0.141	−0.161
Water Level (m)	−0.623	0.157	0.157	0.141	1.000	−0.196
FoS	0.259	0.838	−0.105	−0.161	−0.196	1.000

Table 4. Pearson correlation matrix showing the linear relationships between geotechnical variables and FoS.

$$\begin{aligned} FoS_{(XGB\ Predicted)} &= 83271736324.44 - 164228923.49 \cdot c \\ &+ 1334374999.12 \cdot f + 1053799269.41 \cdot g \\ &- 1181048549.29 \cdot q - 439167047.71 \cdot WL - 0.0002 \cdot c + 9908557340.19 \cdot c \cdot f \\ &- 11148653743.08 \cdot c \cdot g - 6982405578.41 \cdot c \cdot q - 3438887076.71 \cdot c \cdot WL \\ &+ 0.0019 \cdot f - 14035662985.94 \cdot f \cdot g - 5820841941.29 \cdot f \cdot q + 14877604587.24 \cdot f \cdot WL \\ &- 0.0002 \cdot g + 38799142502.49 \cdot g \cdot q - 5480189076.37 \cdot g \cdot WL \\ &+ 0.0000 \cdot q - 22807627661.18 \cdot q \cdot WL - 0.0045 \cdot WL \end{aligned} \tag{4}$$

Where, $R^2 = 0.88$ and RMSE = 0.12.

This newly developed second-order polynomial correlation, fitted to the XGBoost model output, demonstrates exceptional predictive capability with an R^2 value of 0.88 and an RMSE of only 0.12. Compared to the previously derived RF and OLS models, which had R^2 values of 0.75 and 0.83 respectively, this surrogate provides a significantly more accurate approximation of the FoS. The enhanced performance is attributed to the XGBoost model's ability to capture complex nonlinear interactions, which are then preserved and symbolically represented through the polynomial regression. This makes the new correlation both interpretable and highly precise, offering a robust tool for geotechnical design and analysis.

It is evident that none of the model predictions perfectly align with this ideal line. The RF and OLS predictions generally overestimate the FoS values across the range, while the XGBoost model exhibits significant non-linear deviations, especially at higher values. These discrepancies indicate that the derived correlation equations require further adjustment and calibration to improve their accuracy and bring the model predictions into closer agreement with the actual FoS values ultimately achieving better alignment with the 1:1 reference line. This is essential for improving model reliability in geotechnical design and safety analysis. The adjusted linear correlations 5, 6 and 7 shown below were developed to improve the agreement between predicted and actual FoS values by calibrating the original model outputs using simple linear regression post-processing. Specifically, the predicted FoS values from the RF, OLS, and XGBoost models were individually regressed against the corresponding actual FoS values from the dataset to establish direct linear mapping equations of the form; $FoS_{actual} = a \cdot FoS_{pred} + b$. Following are the adjusted correlations for all the three methods:

1. Random Forest (RF):

$$\begin{aligned} FoS_{adjusted} &= 0.5421 \cdot FoS_{(RF\ predicted)} + 0.5067 \\ R^2 &= 0.902,\ RMSE = 0.092 \end{aligned} \tag{5}$$

2. OLS Regression:

$$\begin{aligned} FoS_{adjusted} &= 1.2836 \cdot FoS_{(OLS\ predicted)} - 0.5197 \\ R^2 &= 0.922,\ RMSE = 0.072 \end{aligned} \tag{6}$$

3. XGBoost (Polynomial):

$$\begin{aligned} oS_{adjusted} &= 1.2836 \cdot FoS_{(XGB\ predicted)} + 1.1239 \\ R^2 &= 0.958,\ RMSE = 0.067 \end{aligned} \tag{7}$$

This calibration step effectively adjusts the model outputs to better reflect the real trend and scale observed in the actual measurements. The resulting equations significantly improve the alignment with the ideal 1:1 line, as evidenced by the high coefficients of determination (R^2 values exceeding 0.95) and low RMSE values as shown in Fig. 8.

Table 5 shows the details of R^2 and RMSE for all the three methods, and the Fig. 9 shows the percent improvement in R^2 and reduction in RMSE.

The bar graph presents a comparative analysis of the performance of three regression methods, RF, OLS, and XGBoost based on their predicted and adjusted R^2 and RMSE values. The upper panel illustrates that R^2 values increase progressively from RF to XGBoost, indicating improved model fit, with adjusted R^2 values showing further refinement, particularly for the XGBoost method which achieves the highest value of 0.96. The lower panel displays a corresponding decrease in RMSE values, demonstrating enhanced prediction accuracy after adjustment. Notably, the adjusted RMSE for RF reduces drastically to 0.010, reflecting a significant calibration improvement. This graphical representation highlights the superior predictive capability and robustness of the XGBoost model, followed by OLS and RF, especially after post-processing or model tuning. The RF method shows the greatest improvement in R^2, increasing from 0.75 to 0.90. This significant enhancement reflects the strong effect of post-processing or model adjustment in boosting the model's explanatory power. Although XGBoost achieves the highest final R^2 value (0.96), its improvement margin is smaller (from 0.88 to 0.96), indicating that it was already well-calibrated in its raw prediction. Similarly, RF exhibits the largest decrease in RMSE, dropping from 0.25 to 0.10, an improvement of 0.15. This suggests a notable reduction in prediction error after adjustment. XGBoost, while having the lowest final RMSE (0.040), shows a relatively smaller improvement (0.08), again due to its already optimized performance prior to adjustment. RF benefits the most from adjustment in terms of

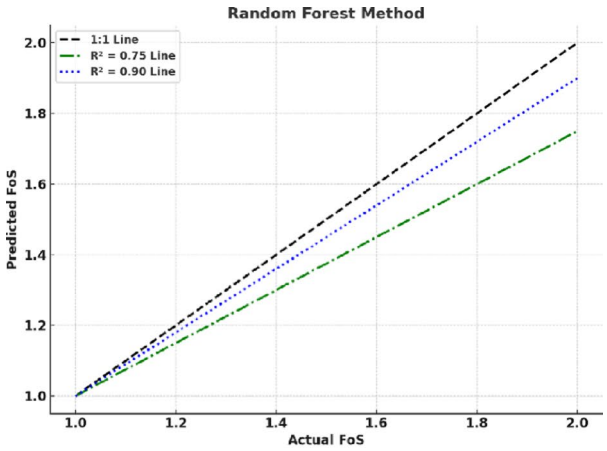

(a) RF

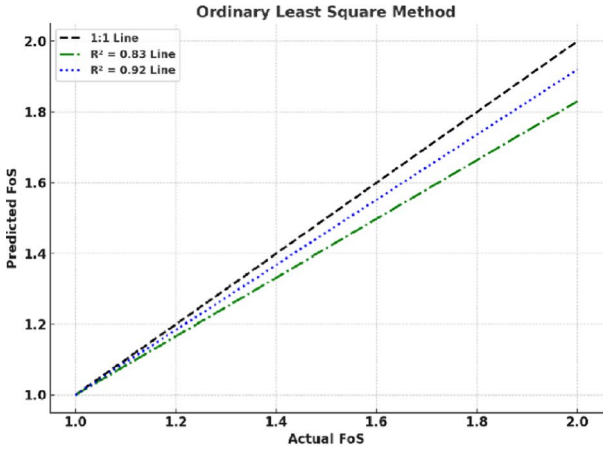

(b) OLS

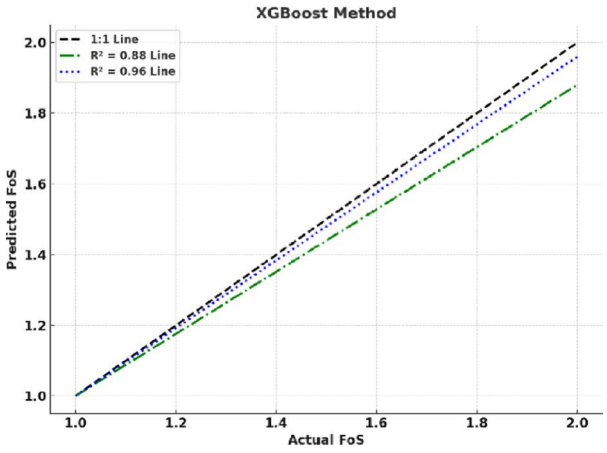

(c) XGBoost

Fig. 8. Plots comparing the actual FoS values against the predicted FoS values for the predicted and adjusted correlations: (**a**) RF, (**b**) OLS, and (**c**) XGBoost.

both R^2 and RMSE. Similarly, XGBoost demonstrates the best absolute performance with highest R^2 and lowest RMSE, but shows less relative improvement.

Limitations of the present study

Despite the robust performance of the developed machine learning surrogate models, this study has several limitations. The models were trained on a dataset generated from a single case study of completely weathered

Method	R^2 Predicted	R^2 Adjusted	% Improvement	RMSE predicted	RMSE adjusted	% Improvement
RF	0.75	0.90	0.15	0.25	0.10	0.15
OLS	0.83	0.92	0.090	0.17	0.080	0.090
XGBoost	0.88	0.96	0.080	0.12	0.040	0.080

Table 5. Summary of predicted and adjusted R^2 and RMSE values for different regression methods.

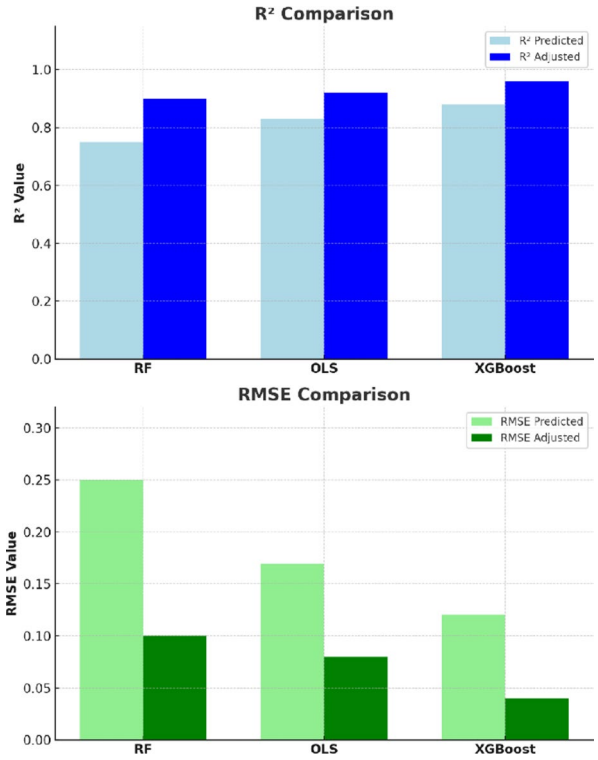

Fig. 9. Comparison of predicted and adjusted R^2 and RMSE across regression methods.

granite, which may limit their generalizability to slopes with different geological formations. The analysis considered static loading conditions and a simplified hydrogeological model, not accounting for dynamic triggers like seismic activity or the full complexity of transient rainfall infiltration and non-Darcian flow in slip zones. Furthermore, the practical application of the sophisticated XGBoost-derived correlation is constrained by its complexity and limited interpretability. Finally, the models are reliable for interpolation within the trained parameter ranges, but their performance for extrapolation remains unverified, and caution is advised when applying them to scenarios beyond the studied conditions.

Conclusions

This study developed an innovative, AI-enhanced framework for slope stability analysis by integrating finite-element-based numerical simulation with machine learning regression. Using the real-world case of the Meizhou landslide, a comprehensive parametric dataset was generated under varying groundwater conditions, capturing key interactions between geotechnical properties and slope stability. Three ML models—RF, OLS, and XGBoost—were trained to predict the factor of safety and produce interpretable surrogate equations suitable for engineering use. Post-regression calibration substantially improved prediction accuracy, with XGBoost achieving superior performance (R^2=0.96, RMSE = 0.040). The analysis underscored the critical influence of water level fluctuations and material strength parameters, particularly cohesion and friction angle, on stability outcomes. The proposed hybrid framework offers a scalable, data-driven tool for rapid slope safety evaluation in rainfall-prone regions, demonstrating notable efficiency over conventional methods. For broader adoption, future work should extend this approach to diverse soil types and dynamic loading scenarios such as seismic events, and adapt it for real-time slope monitoring systems.

Data availability

The supplementary files include the GeoStudio analysis, Annex 1 as mentioned in the manuscript and the Python code based on which the correlations/equations are developed. The files in the GeoStudio folder can be opened using GeoStudio software. They are software based files and can be opened using the mentioned software only.

Received: 10 August 2025; Accepted: 17 December 2025
Published online: 03 January 2026

References

1. Ng, C. W. W., Wang, Y., Zhang, S. & Zhang, Q. Effects of climate change on soil embankments for transport infrastructure. *Transp. Geotechnics*. **48**, 101324 (2024).
2. Abdulahi, M. M. & Egli, P. E. *Landslides Triggered by the July 21–22, 2024, Heavy Rainfall in the Gofa Zone, Southern Ethiopia* (Springer, 2024).
3. Das, R. *Catastrophic Landslide in Wayanad District of Kerala, India on July 30, 2024: A Complex Interplay between geology, geomorphology, and Climate* (Springer, 2024).
4. Vision, W. https://www.worldvision.org/disaster-relief-news-stories/landslides-facts-how-to-help (2024).
5. REUTERS. https://www.reuters.com/business/environment/remnants-typhoon-gaemi-trigger-flash-floods-northeast-china-2024-07-28/ (2024).
6. USGS. https://www.usgs.gov/programs/landslide-hazards/science/2024-hurricane-helene-landslide-hazards (2024).
7. OCHA. https://www.unocha.org/publications/report/pakistan/pakistan-monsoon-2024-flash-update-1-latest-monsoon-developments-and-response-efforts-01-august-2024 (2024).
8. Zhou, C. et al. Catastrophic landslide triggered by extreme rainfall in Chongqing, china: July 13, 2020, Niuerwan landslide. *Landslides* **19** (10), 2397–2407 (2022).
9. Khan, M. I., Fei, J., Chen, X. & Chen, Y. Usage of permeability ratio to check the stability of a pile-soil model with retaining wall support–Huizhou slope failure as a case study. *Int. J. Geo-Engineering*. **16** (1), 7 (2025).
10. Khan, M. I. & Wang, S. Initial risk assessment to find risky slopes. *J. Appl. Sci. Eng.* **26** (11), 1597–1608 (2023).
11. Khan, M. I. Correlations between factor of safety with distributed load and crest length–Zariwam landslide as case study. *Geol. Ecol. Landscapes*. **9** (1), 80–93 (2025).
12. Khan, M. I., Wang, S., Wang, P. & Nikjow, M. A. Soil slope analysis to develop useful correlations in saturated and unsaturated conditions. Proceedings of the Institution of Civil Engineers-Forensic Engineering. **177** (1), 14–22. (2024).
13. Khan, M. I. & Wang, S. Dynamic deformation analysis of the upstream and downstream slope of the rockfill nauseri dam. *J. Appl. Sci. Eng.* **26** (2), 293–301 (2022).
14. Khan, M. I. & Wang, S. Develop correlations between soil parameters: Jandola Pakistan landslide as case study. Proceedings of the Institution of Civil Engineers-Forensic Engineering. ;**175**(3):78–86. (2022).
15. Khan, M. I. & Wang, S. Correlating groundwater level and shear strength: Kotkai Pakistan landslide as case study. Proceedings of the Institution of Civil Engineers-Forensic Engineering. ;**175**(1):21 – 7. (2022).
16. Khan, M. I. & Wang, S. Slope stability analysis to correlate shear strength with slope angle and shear stress by considering saturated and unsaturated seismic conditions. *Appl. Sci.* **11** (10), 4568 (2021).
17. Khan, M. I. & Wang, S. Slope stability analysis to develop correlations between different soil parameters and factor of safety using regression analysis. *Pol. J. Environ. Stud.* **30**(5), 4021-4030 (2021).
18. Wang, S. & Khan, M. I. Developing correlations for advance prediction of slope factor of safety using linear regression analysis–Karachi landslide as a case study. *Pol. J. Environ. Stud.* **30** (6), 5849–5862 (2021).
19. Khan, M. I. & Wang, S. Method for predicting factor of safety and seepage due to variation in dam width and other parameters. Proceedings of the Institution of Civil Engineers-Geotechnical Engineering. ;176(2):157 – 65. (2023).
20. Dille, A. et al. Causes and triggers of deep-seated hillslope instability in the tropics–Insights from a 60-year record of Ikoma landslide (DR Congo). *Geomorphology* **345**, 106835 (2019).
21. Puente-Sotomayor, F., Egas, A. & Teller, J. Land policies for landslide risk reduction in Andean cities. *Habitat Int.* **107**, 102298 (2021).
22. Abella, E. A. C. & Van Westen, C. J. Qualitative landslide susceptibility assessment by multicriteria analysis: A case study from San Antonio Del Sur. *Guantánamo Cuba Geomorphology*. **94** (3–4), 453–466 (2008).
23. Panchal, S. & Shrivastava, A. K. Landslide hazard assessment using analytic hierarchy process (AHP): A case study of National highway 5 in India. *Ain Shams Eng. J.* **13** (3), 101626 (2022).
24. Singh, K. & Kumar, V. Hazard assessment of landslide disaster using information value method and analytical hierarchy process in highly tectonic Chamba region in bosom of himalaya. *J. Mt. Sci.* **15** (4), 808–824. https://doi.org/10.1007/s11629-017-4634-2 (2018).
25. Wang, P. et al. GIS-based random forest weight for rainfall-induced landslide susceptibility assessment at a humid region in Southern China. *Water* **10** (8), 1019 (2018).
26. Zhang, T. et al. Improved tree-based machine learning algorithms combining with bagging strategy for landslide susceptibility modeling. *Arab. J. Geosci.* **15** (2), 183 (2022).
27. Tao, Z. et al. Physical model test study on shear strength characteristics of slope sliding surface in Nanfen open-pit mine. *Int. J. Min. Sci. Technol.* **30** (3), 421–429 (2020).
28. Li, T. et al. Automated machine learning for rainfall-induced landslide hazard mapping in Luhe County of Guangdong Province, China. *China Geol.* **7** (2), 315–329 (2024).
29. Huang, F. et al. Influence of heavy rainfall and different slope cutting conditions on stability changes in red clay slopes: a case study in South China. *Environ. Earth Sci.* **81** (15), 384. https://doi.org/10.1007/s12665-022-10466-x (2022).
30. Dou, H., Huang, S., Wang, H. & Jian, W. Repeated failure of a high cutting slope induced by excavation and rainfall: A case study in Fujian, Southeast China. *Bull. Eng. Geol. Environ.* **81** (6), 227 (2022).
31. Ran, Q., Qian, Q., Wang, G. & Fu, X. Su D-y. Analytical solution for slope instability assessment considering impact of confined aquifer. *J. Cent. South. Univ.* **22** (4), 1502–1509 (2015).
32. Yu, L. et al. Analysis of the mechanism and failure mode of landslides subjected to transient seepage in a Piedmont region of Nanjing area. *Bull. Eng. Geol. Environ.* **80** (10), 7441–7456 (2021).
33. Chen, Y., Withanage, K. R., Uchimura, T., Mao, W. & Nie, W. Shear deformation and failure of unsaturated sandy soils in surface layers of slopes during rainwater infiltration. *Measurement* **149**, 107001 (2020).
34. Rao, Y., Chen, H., Yang, T. & Zhang, Z. Experiments and analytical method for landslide scarp caused by water-induced weakening of basal sliding zone. *Acta Geotech.* 19 (9), 5873-5890 (2024).
35. Rao, Y., Zhang, Z., Yang, T. & Chen, H. A new theoretical model to locate the back scarp in landslides caused by strength reduction in slip zone soil. *Comput. Geotech.* **159**, 105410 (2023).
36. Cui, H., Ji, J., Hürlimann, M. & Medina, V. Probabilistic and physically-based modelling of rainfall-induced landslide susceptibility using integrated GIS-FORM algorithm. *Landslides* **21** (6), 1461–1481 (2024).
37. Cui, H-Z., Tong, B., Wang, T., Dou, J. & Ji, J. *A Hybrid data-driven Approach for rainfall-induced Landslide Susceptibility Mapping: Physically-based Probabilistic Model with Convolutional Neural Network* (Journal of Rock Mechanics and Geotechnical Engineering, 2024).
38. Vickneswaran, T. & Ravichandran, N. Stability and deformation responses of Earth slopes subjected to multiple natural and manmade hazards. *Int. J. Geomech.* **22** (3), 04021304 (2022).
39. Wang, Q. et al. Insight into the permeability and microstructure evolution mechanism of the sliding zone soil: a case study from the Huangtupo Landslide, three Gorges Reservoir, China. *J. Earth Sci.* **35** (3), 941–954 (2024).

40. Liu, Z. et al. Toward the reliable prediction of reservoir landslide displacement using earthworm optimization algorithm-optimized support vector regression (EOA-SVR). *Nat. Hazards.* **120** (4), 3165–3188. https://doi.org/10.1007/s11069-023-06322-1 (2024).
41. Guo, L., He, K., Liu, H., Meng, F. & Wang, X. Physical prediction model of compound hydrodynamic unload-load response ratio and its application in reservoir colluvium landslide. *J. Earth Sci.* **35** (4), 1304–1315. https://doi.org/10.1007/s12583-022-1662-9 (2024).
42. Tang, H., Li, C. & Gong, W. Fundamental attribute and research approach of landslide evolution. *Earth Sci.* **47** (12), 4596–4608 (2022).
43. Zhang, L., Wu, F., Zhang, H., Zhang, L. & Zhang, J. Influences of internal erosion on infiltration and slope stability. *Bull. Eng. Geol. Environ.* **78** (3), 1815–1827. https://doi.org/10.1007/s10064-017-1185-2 (2019).
44. Chandel, A., Singh, M. & Thakur, V. Empirical solution for predicting soil rim slope deformation under Cyclic reservoir water level fluctuations. *Geotech. Geol. Eng.* **42** (8), 7655–7675. https://doi.org/10.1007/s10706-024-02944-9 (2024).
45. Tan, Y. et al. Slope stability analysis of saturated–unsaturated based on the GEO-studio: a case study of Xinchang slope in Lanping County, Yunnan Province, China. *Environ. Earth Sci.* **82** (13), 322. https://doi.org/10.1007/s12665-023-11006-x (2023).
46. Yu, X., Zhao, T., Gong, B. & Tang, C. The water weakening effect on the progressive slope failure under excavation and rainfall conditions. *Bull. Eng. Geol. Environ.* **83** (8), 316. https://doi.org/10.1007/s10064-024-03809-4 (2024).
47. Huang, Q., Wang, J., Kulatilake, P. H. S. W., Guo, H. & Shen, J. Interpreting the formation mechanism of a complex landslide: a case study of a reactivated landslide of a reinforced embankment slope. *Bull. Eng. Geol. Environ.* **82** (12), 472. https://doi.org/10.1007/s10064-023-03492-x (2023).
48. Paudyal, P., Dahal, P., Bhandari, P. & Dahal, B. K. Sustainable rural infrastructure: guidelines for roadside slope excavation. *Geoenvironmental Disasters.* **10** (1), 11. https://doi.org/10.1186/s40677-023-00240-x (2023).
49. Chen, J. et al. Study on pore size effect of low permeability clay seepage. *Arab. J. Geosci.* **12**, 1–10 (2019).
50. Zhong-qi, Y. & Qian, X. Fundamental drawbacks and disastrous consequences of current geotechnical safety design theories for slopes. *Chin. J. Geotech. Eng.* **36** (9), 1601–1606 (2014).
51. Pei, T. & Qiu, T. Machine learning with monotonic constraint for geotechnical engineering applications: an example of slope stability prediction. *Acta Geotech.* **19** (6), 3863–3882 (2024).
52. Zhang, W., Wu, C., Zhong, H., Li, Y. & Wang, L. Prediction of undrained shear strength using extreme gradient boosting and random forest based on bayesian optimization. *Geosci. Front.* **12** (1), 469–477 (2021).
53. Chen, W., Zhong, C., Qin, X. & Wang, L. Deep learning based landslide susceptibility assessment. Intelligent Interpretation for Geological Disasters: from Space-Air-Ground Integration Perspective. 137 – 69. (Springer, 2023).
54. Yadav, D. K., Chattopadhyay, S., Tripathy, D. P. & Mishra, P. SinghEnhanced slope stability prediction using ensemble machine learning techniques. *Sci. Rep.* **15** (1), 7302 (2025).
55. Zhong, K. et al. Prediction of slope failure probability based on machine learning with genetic-ADASYN algorithm. *Eng. Geol.* **346**, 107885 (2025).
56. Onyelowe, K. C., Ebid, A. M., Hanandeh, S. & Kamchoom, V. Evaluating the slope behavior for geophysical flow prediction with advanced machine learning combinations. *Sci. Rep.* **15** (1), 6531 (2025).
57. Lin, S. et al. A comprehensive evaluation of ensemble machine learning in geotechnical stability analysis and explainability. *Int. J. Mech. Mater. Des.* **20** (2), 331–352 (2024).
58. Jing, Y. et al. Factor of safety prediction for slope stability using PCA and BPNN in guangdong's H mining area. *Sci. Rep.* **15** (1), 12804 (2025).
59. Liu, G., Zhou, Z., Xu, S. & Mi, W. Hysteresis of dam slope safety factor under water level fluctuations based on the LEM coupled with FEM method. *CMES-Computer Model. Eng. Sci.* **133**, 1285–1303 (2022).
60. Jalal, F. E., Xu, Y., Iqbal, M., Javed, M. F. & Jamhiri, B. Predictive modeling of swell-strength of expansive soils using artificial intelligence approaches: ANN, ANFIS and GEP. *J. Environ. Manage.* **289**, 112420 (2021).
61. Siddiqui, F. I. & Osman, S. B. A. B. S. Simple and multiple regression models for relationship between electrical resistivity and various soil properties for soil characterization. *Environ. Earth Sci.* **70**, 259–267 (2013).
62. Kumar, N. & Kumari, S. Slope stability analysis of vetiver grass stabilized soil using genetic programming and multivariate adaptive regression splines. *Transp. Infrastructure Geotechnology*. **11** (5), 3558–3580 (2024).
63. Sun, J. et al. Slope-scale landslide susceptibility assessment based on coupled models of frequency ratio and multiple regression analysis with limited historical hazards data. *Nat. Hazards.* **120** (1), 1–23 (2024).
64. Zhongqi, Y. Study on the instability condition and landslide mechanism of subgrade slope in Mei–Da expressway. *Chin. J. Geol. Hazard. Control.* **35** (4), 1–12 (2024).
65. NEWS B. (2024). https://bnonews.com/index.php/2024/05/highway-collapses-in-southern-china-killing-at-least-24-people/
66. Knill, J. *Report on the Shum Wan Road Landslide of 13 August 1995: Volume 1–Independent Review of the Investigation by the Geotechnical Engineering Office* (Geotechnical Engineering Office, 1996).
67. Geoguide, I. Guide to retaining wall design. Geotechnical engineering office, Civil engineering department, Hong Kong. (1993).
68. Kim, D., Kim, T., Kim, Y., Byun, Y-H. & Yun, T. S. A ChatGPT-MATLAB framework for numerical modeling in geotechnical engineering applications. *Comput. Geotech.* **169**, 106237 (2024).

Acknowledgements

The authors gratefully acknowledge Shenzhen University for providing laboratory facilities, computational resources, and a collaborative research environment. Special thanks to the College of Civil and Transportation Engineering for their continuous academic and technical support throughout this study.

Author contributions

Muhammad Israr Khan : Conceptualization, Methodology, Software, Formal analysis, Investigation, Data curation, Visualization, Writing – original draft, Writing – review & editingJianbo Fei : Supervision, Conceptualization, Funding acquisitionXiangsheng Chen : Funding acquisitionMuhammad Hamza : Investigation, Writing – review & editing.

Funding

The research is funded by the National Natural Science Foundation of China (No. 52422807).

Declarations

Competing interests

The authors declare no competing interests.

Additional information

Supplementary Information The online version contains supplementary material available at https://doi.org/10.1038/s41598-025-33324-9.

Correspondence and requests for materials should be addressed to J.F.

Reprints and permissions information is available at www.nature.com/reprints.

Publisher's note Springer Nature remains neutral with regard to jurisdictional claims in published maps and institutional affiliations.